CHINA FOUNDRY Research & Development
Vol.16 No.6 November 2019
https://doi.org/10.1007/s41230-019-9068-8

Effect of pouring and cooling temperatures on microstructures and mechanical properties of as-cast and T6 treated A356 alloy

***Xin-ping Hu[1], Yang Zhao[1], Qing Wang[1], Xue-zhi Zhang[2], Rui-xin Li[1] and Bing-rong Zhang[1]**

1. School of Mechanical Engineering, Qilu University of Technology, Jinan 250353, China

2. Hebei Champion Target Technology Co., Ltd., Xinji 056320, China

Abstract: The A356 castings were fabricated using a well-developed temperature controlled permanent mold. To improve the strength and hardness of cast A356, the microstructures and mechanical properties of as-cast and T6 heat treated A356 alloy with various mold and pouring temperatures were studied. The results reveal that the undercooling is closely related to the mold and pouring temperatures. As the mold/pouring temperature changed from 258 °C / 680 °C and 270 °C / 680 °C to 288 °C / 650 °C, the in-situ undercooling is 12 °C, 17 °C and 11 °C, respectively. It is observed that the Si phase changes from long continuous flake to discontinuous globular-fibrous morphology after T6 heat treatment as the mold and pouring temperature is 270 °C / 680 °C, and the T6 heat treated specimens exhibit better mechanical properties in comparison to those as-cast ones with an increase of 162% and 102% in yield strength and elongation, which are 34.6% and 190% higher than the ASTM B108-03a standard, respectively. As a result, the tensile fracture morphology of the as-cast A356 alloy shows quasi-cleavage fracture and the T6 heat treated A356 alloy shows ductile fracture.

Key words: solidification; microstructure; permanent mold; T6 heat treatment; A356

CLC numbers: TG146.21 **Document code:** A **Article ID:** 1672-6421(2019)06-380-06

A356 is a hypoeutectic Al-Si alloy which has been widely used in many industrial fields owing to its good castability, low density, high corrosion resistance, and good weldability [1-3]. The T6 heat treated A356 has often been used in automobile wheel hubs [4-5]. In order to achieve good comprehensive performance, the most common method is adding less than 0.2wt.% of Ti to the Al-Si alloy to refine the grain size and obtain a fine-equiaxed structure. Al_3Ti and α-Al have similar lattice constants, so the Al_3Ti particles act as heterogeneous nucleation sites for α-Al grains and refine the microstructure of A356 [6,7]. However, a previous researcher found that the Al_3Ti particles can only dissolve into liquid alloy at high temperature, which significantly deteriorates its refining effect [8,9].

As it was known, the mechanical properties of A356 are largely dependent on the size and morphology of eutectic Si phase. The T6 heat treatment can help the eutectic Si change from coarse long flake or acicular form to fine globular-fibrous or spheroidal morphology [10-12]. Many researchers owed this improvement to the presence of magnesium, in which Mg reacts with Si to form Mg_2Si, the precipitation hardening phase [13,14]. During T6 heat treatment, two traditional stages are involved. The first stage is called solid solution treatment and quenching, and the second stage is called artificial aging. Those processes change the morphology of the strengthening phases and improve the ductile property of A356 [15].

Microstructures and mechanical properties are also dependent on parameters of the casting process. Although pouring and mold temperatures are two important casting parameters to produce high quality and low porosity castings [16,17], there are limited studies showing the effects of pouring temperature, mold temperature, mold cooling conditions on the performance of A356 in permanent mold casting. In this study, in order to study the effect of specific cooling conditions on the microstructure and mechanical properties of the A356, a temperature controlled permanent mold is developed to fabricate A356 castings. The microstructures and mechanical properties of as-cast and T6 heat treated alloys are investigated.

***Xin-ping Hu**

Male, born in 1969, Ph.D., Professor. His research interests mainly focus on solidification, high performance Al cast alloys and mold designing.

E-mail: huxxpp@qlu.edu.cn

Received: 2019-05-22; Accepted: 2019-09-10

1 Experimental procedure

The material used was a commercial A356 alloy with a chemical composition of 6.5%–7.5% Si, 0.3%–0.45% Mg, less than 0.2% Ti. After the alloy was melted in a crucible inside the electric resistance furnace, it was poured into the mold cavity of 10 mm in diameter, and the specimen dimensions are based on the standard of GB/T 228-2002. A data acquisition and mold heating system is shown in Fig. 1, which is equipped to control the temperature of permanent mold prior to the pouring process, and to record the temperature change of the mold cavity and the casting during the cooling process. In Fig. 1, a thermocouple connected with the temperature recorder is inserted in the top of mold cavity to record the temperature of the mold cavity before the filling process, and the cooling temperature of the casting after filling. A heater with four terminals is imbedded in the heating plate to heat the permanent mold. A temperature controller connected to the alternating current (AC) contactor is employed to adjust the mold temperature.

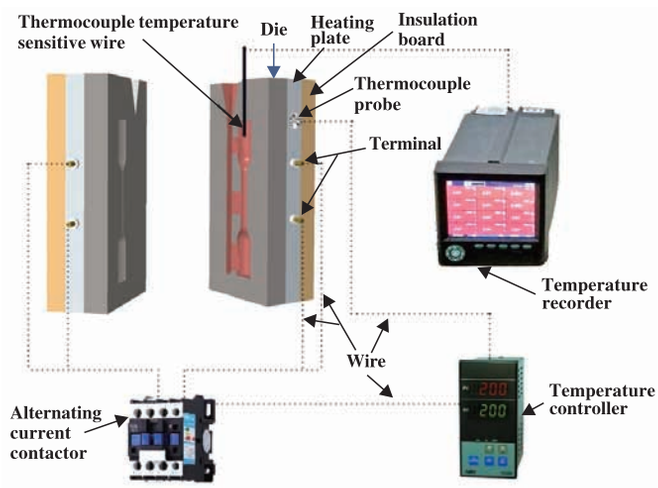

Fig. 1: Schematic of mold temperature controller and temperature recorder

Three sets of specimens were fabricated at different pouring and mold temperatures, as shown in Table 1. After tensile tests, the specimens were cut into samples for microstructure analysis and hardness testing. The microstructure analysis samples were polished and further etched with Keller's reagent. The microstructures were revealed by a Hitachi Regulus 8220 electron microscope and a Leica DM2700M optical microscope. The secondary dendrite arm spacing (SDAS) was measured by using micrographs with an accurate scale bar with the help of image processing software. Lines parallel to the direction of primary growth were drawn and then the SDASs were measured by averaging the distance between adjacent side branches on the longitudinal section of a primary dendrite [18]. The Brinell hardness was tested by a XHB-3000 hardness tester with a 5 mm diameter cemented carbide ball under a load of 1,250 N for 30 s. Vickers hardness was obtained by HXD-1000TMC tester under a load of 0.025 N for 30 s. The tensile test was conducted on an universal testing machine CHT4605. T6 heat treatment was carried out in an anti-oxidation atmosphere furnace TCXQ-1700, and conducted with the procedure shown in Fig. 2.

Table 1: Casting conditions of three sets of specimens

Samples	Mold temperature (°C)	Pouring temperature (°C)
T258	258	680
T270	270	680
T288	288	650

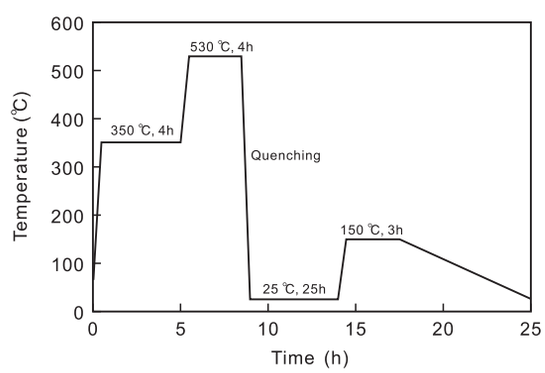

Fig. 2: T6 heat treatment procedure for A356 alloy

2 Results and discussion

2.1 Temperature-time curves

Three temperature-time curves are shown in Fig. 3. In order to present striking contrast between different pouring times, the curves from 301 s to 335 s are amplified, and are shown in the upper right hand corner of the graph. Before 301 s, the mold cavity temperature is recorded, and after 301 s, the casting temperature is recorded. In order to decrease the temperature drop as much as possible, the liquid alloy is poured into the cavity within 3 s after the crucible was taken out of the furnace. It is well known that undercooling influences the microstructure and mechanical properties. For hypoeutectic Al-7% Si alloy, the theoretical solidification range is from 602 to 577 °C according

to the Al-Si phase diagram, and its eutectic undercooling (ΔT_{eut}) could be determined by the equation below, according to the modified Jackson-Hunt model [20]:

$$\Delta T_{eut} = (1+\varphi)\frac{k_2}{\lambda_2} \quad (1)$$

where, φ is a dimensionless parameter, and the value of φ was found to be 2.3 for Al-Si alloys; and k_2 is material parameter constant related to thermodynamic parameters such as diffusion coefficient, liquidus slope in phase diagram, Gibbs-Thompson coefficient, etc.; λ_2 is the secondary dendrite arm spacing related to the cooling rate in solidification or solidification time.

For a typical eutectic phase diagram alloy, there are two slope transitions in the cooling temperature-time curve during solidification. One is the time when temperature decreases to liquidus, and the other is the time when temperature decreases to solidus. In the upper right hand corner of Fig. 3, the graph shows the temperature of liquid alloy decreases to below 610 °C quickly and starts to solidify. It is hard to distinguish the temperature-time curve's first slope change in the beginning of solidification, but the second slope change occurs at temperatures 565, 560 and 566 °C for T258, T270 and T288 curves, respectively. So, during the solidification process in a temperature controlled permanent mold of A356, the in-situ undercooling temperature is 12, 17 and 11 °C, respectively, which is calculated based on the differences between the eutectic temperature (577 °C) and the temperatures of the turning point on the solidification curves (565, 560 and 566 °C). An

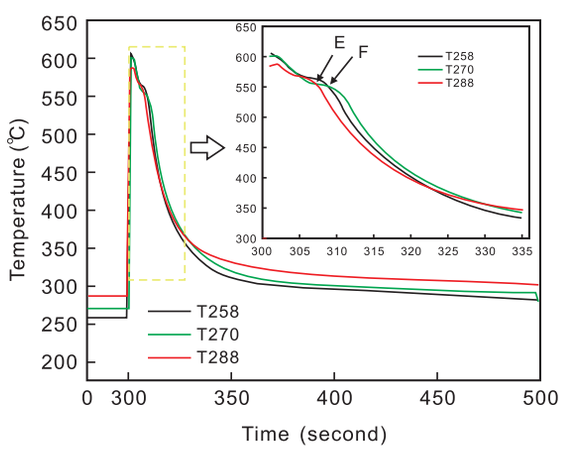

Fig. 3: Mold cavity temperature (casting temperature) versus time curves

interesting puzzle is presented that the curves T270 and T258 have two characteristic points, E and F, after pouring within 10 s. Within one second after pouring, the T270 and the T258 drop quickly, and they have the similar cooling rate until they separate from each other at about 5 s (Point E) after pouring, and then the T270 is below the T258. When they intersect at F (about 8 s after pouring), the T270 is above the T258 again. This could be explained as follows: First, because of the low mold temperature of T258, the temperature of the liquid metal drops rapidly and solidifies rapidly after pouring. In the initial stage of solidification, the amount of solidified Al alloy of the T258 is more than that of T270. Therefore, more solidification latent heat of the T258 should be released and the cooling rate is slower than that of the T270, then the T270 becomes below the T258. Obviously, the solidification time of the T270 is longer than that of T258, and when the solidification is about to finish and the latent heat of solidification is almost released, the T270 gradually exceeds the T258, and then the T270 becomes above of the T258.

Because of the relative higher mold temperature and lower pouring temperature, the T288 curve is below that of the T258 and T270 in the beginning of solidification within 26 s after pouring and then reaches above of them. Since T270 is the most widely used condition in the automotive industry such as in the production of A356 automobile wheel hubs, it was chosen to carry out the analysis below.

2.2 Microstructure

In order to study the relationship between the cooling rate, microstructure, and property, three zones were studied which were selected at the distance of 0 R, 0.5 R and R from the center of the sample T270, where R is the radius of the sample. The microstructures are shown in Fig. 4. The microstructure refinement could be evaluated by the value of secondary dendrite arm spacing (SDAS, λ_2), which is related to the cooling rate as discussed above. Based on the inverse relationship between solidification time (t_f) and cooling rate, it could be predicted by an empirical expression [21-23]:

$$\lambda_2 = B \times t_f^{(n)} \quad (2)$$

where, B and n are constants related to materials and solidifying condition.

However, it is difficult to determine the in-situ solidification time according to the temperature vs. time curves above. The

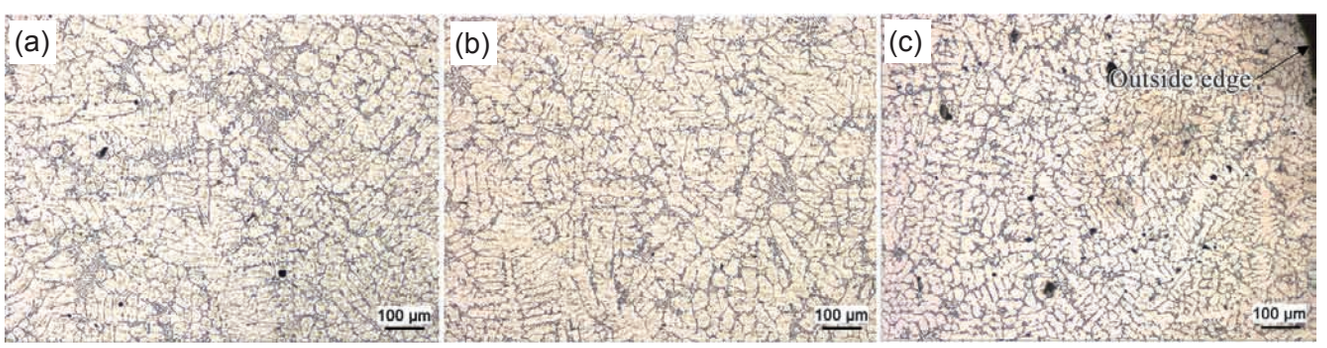

Fig. 4: Microstructures of as-cast A356 in different positions from center to surface: (a) 0 R; (b) 0.5 R; (c) R

imitation of solidification has been carried out, and the t_f is 0.25, 0.2 and 0.1 s, respectively, for samples located at 0 R, 0.5 R and R from the center, and the measured SDASs are 19.35, 19.13, and 16.65 μm, respectively. The constants B and n are 24.793, 0.171, and therefore, the fitting curve is shown in Fig. 5.

After T6 heat treatment, the microstructures of the sample at 0 R, 0.5 R and R from the center are shown in Fig. 6. An image processing software is applied to analyze the images in Fig. 4 and Fig. 6 to show the difference of their microstructure such as the grain size and distribution. The detailed analysis procedures can be found in reference [24]. The calculated results are listed in Table 2.

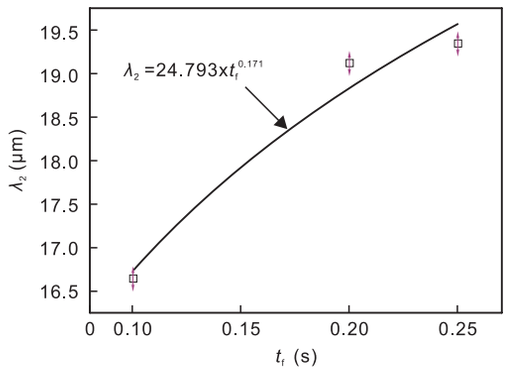

Fig. 5: Fitting curve of SDAS (λ_2) and solidification time (t_f)

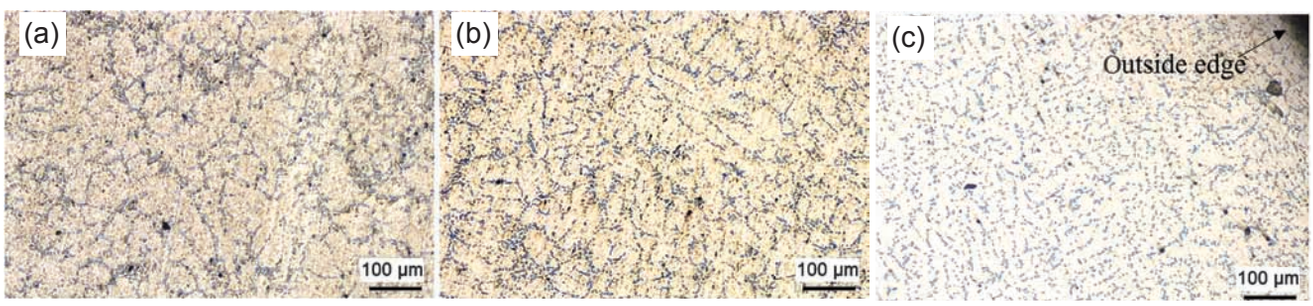

Fig. 6: Microstructures of T6 heat treatment A356 in different locations from center to surface: (a) 0 R; (b) 0.5 R; (c) R

Table 2: Characteristics of α-Al grains and SDAS in Fig. 4 and Fig. 6

	As-cast			T6		
	0 R	0.5 R	R	0 R	0.5 R	R
SDAS (μm)	19.35	19.13	16.65	25.72	25.66	20.44
Total object number	1001	923	1317	622	828	998
Mean aspect ratio	2.06	2.11	2.02	1.87	2.00	2.13
Mean area (μm^2)	775.18	774.97	544.10	1278.34	946.79	767.63
Mean diameter (μm)	28.90	29.96	25.50	37.19	32.15	30.18

It is clear that the SDAS is finer near the edge of the specimen, and the mean diameter of α-Al becomes smaller from center to edge for both as-cast and T6 heat treatment A356 specimens. After T6 heat treatment, the α-Al grain becomes bigger because it is heated to high temperature and held for hours to ensure the dissolution of Si phase. In the subsequent quenching and artificial aging processes, the Si precipitates along the α-Al grain boundary with their morphology changing from long continuous flake to discontinuous globular-fibrous morphology.

2.3 Mechanical properties

Hardness and ultimate tensile strength of as-cast and T6 heat treated A356 alloy are shown in Table 3. It could be seen that after T6 heat treatment, the ultimate tensile strength is improved from 140 to 307 MPa, HBW increases from 66 to 88 N·mm^{-2}, elongation increases from 4.3% to 8.7%, microhardness of α-Al increases from HV74.35 to HV104.49, and microhardness of Si phase increases from HV84.50 to HV115.98. The ultimate tensile strength of as-cast specimen is lower than that of the standard ASTM B108-03a. This is due to the lower cooling rate caused by the heating plate and insulation board during solidification which results in the greater value of λ_2 and larger grain size. However, the T6 heat treatment enhanced the values of ultimate tensile strength and elongation greatly, and they are 34.6% and 190% higher than those of the standard ASTM B108-03a, respectively.

2.4 Tensile fracture morphology

The tensile fracture morphologies of the as-cast and T6 heat treated A356 alloy are shown in Fig. 7. In Fig. 7(a), the fracture surface is composed of some typical cleavage fractures and a small number of dimples. There are some thick and smooth cleavage platforms, and some river pattern lines caused by the eutectic silicon phases. For river pattern lines shown in Section I, small and narrow tear edges join together and become a big tear edge. Some parallel secondary cleavage cracks are also observed in some big grains in Section II. Some grains become longer and narrower due to the drawing force. The wide-angle grain boundaries become the obstacles of crack propagation which results in the fan-shaped patterns as shown in Section III.

Table 3: Mechanical properties of as-cast and T6 heat treated A356 comparing to ASTM values

	A356 (This study)		A356 (ASTM B108-03a)	
	As-cast	T6	As-cast	T6
UTS (MPa)	140	307	⩾145	⩾228
YS (MPa)	105	275	⩾69	⩾152
HBW ($N·mm^{-2}$)	66	88	-	85 (typical)
Elongation (%)	4.3	8.7	⩾3	⩾3
HV (α-Al)	74.35	104.49	-	-
HV (Si phase)	84.50	115.98	-	-

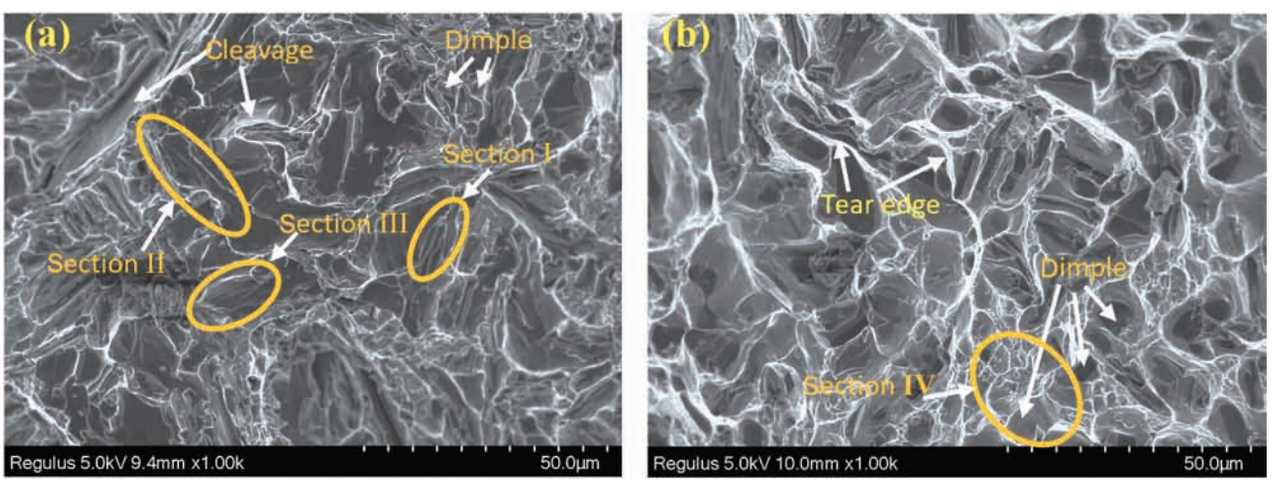

Fig. 7: Tensile fracture morphologies of A356 alloy: (a) as-cast; (b) T6 heat treatment

On the basis of characteristics above, it is concluded that the fracture of as-cast A356 here is quasi-cleavage fracture.

In Fig. 7 (b), small dimples on the surface are observed as shown in Section IV. However, some river pattern lines are also observed. Due to the nature of higher elongation, it could be inferred that the fracture of T6 heat treated A356 is ductile.

3 Conclusions

The effect of pouring and cooling temperatures on the microstructures and mechanical properties of as-cast and T6 heat treated A356 aluminum alloy has been studied. According to the metallographic examination and tensile testing results, the following conclusions can be drawn:

(1) As the mold temperature and pouring temperature changes from 258 °C/680 °C, 270 °C/680 °C to 288 °C/650 °C, the undercooling degree changes from 12 °C, 17 °C to 11 °C.

(2) The secondary dendrite arm spacing of the T270 specimen at 0 R, 0.5 R, and R from the center of the specimen are 19.35 μm, 19.13 μm, and 16.65 μm, respectively, which can be predicted by the empirical expression $\lambda_2=24.793\times t_f^{0.171}$.

(3) After T6 heat treatment for T270 specimen, the Si phase changes from long continuous flake to discontinuous globular-fibrous morphology. The ultimate tensile strength is improved from 140 to 307 MPa, HBW increases from 66 to 88 $N·mm^{-2}$, elongation increases from 4.3% to 8.7%, microhardness on α-Al increases from HV74.35 to HV104.49, and microhardness on Si phase increases from HV84.50 to HV115.98.

(4) The tensile fracture of the as-cast A356 alloy is quasi-cleavage fracture, and the T6 heat treatment A356 alloy is ductile fracture.

References

[1] Youn S W, Kang C G. Characterization of age-hardening behavior of eutectic region in squeeze-cast A356-T5 alloy using nanoindenter and atomic force microscope. Materials Science & Engineering A, 2006, 425: 28–35.

[2] Zhang L Y, Jiang Y H, Ma Z, et al. Effect of cooling rate on solidified microstructure and mechanical properties of aluminum A356 alloy. Journal of Materials Processing Technology, 2008, 207: 107–111.

[3] Lu S P, Du R, Liu J P, et al. A new fast heat treatment process for cast A356 alloy motorcycle wheel hubs. China Foundry, 2018, 15(1): 11–16.

[4] Tebaldini M, Petrogalli C, Donzella G, et al. Estimation of fatigue limit of a A356-T6 automotive wheel in presence of defects. Procedia Structural Integrity, 2017, 7: 521–529.

[5] Wu X, Zhang H, Chen H, et al. Evolution of microstructure and mechanical properties of A356 aluminium alloy processed by hot spinning process. China Foundry, 2017, 14:138–144.

[6] Ma S, Wang Y, Wang X. The in-situ formation of Al_3Ti reinforcing particulates in an Al-7wt.%Si alloy and their effects on mechanical properties. Journal of Alloys and Compounds, 2019, 792: 365–374.

[7] Ozturk I, Agaoglu G H, Erzi E, et al. Effects of strontium addition on the microstructure and corrosion behavior of A356 aluminum alloy. Journal of Alloys and Compounds, 2018, 763: 384–391.
[8] Zhao H, Bai H, Wang J, et al. Preparation of Al-Ti-C-Sr master alloys and their refining efficiency on A356 alloy. Materials Characterization, 2009, 60: 377–383.
[9] Pramod S L, Ravikirana, Rao A K P, et al. Effect of Sc addition and T6 aging treatment on the microstructure modification and mechanical properties of A356 alloy. Materials Science and Engineering: A, 2016, 674: 438–450.
[10] Haskel T, Verran G O, Barbieri R. Rotating and bending fatigue behavior of A356 aluminum alloy: Effects of strontium addition and T6 heat treatment. International Journal of Fatigue, 2018, 114: 1–10.
[11] Elahi M A, Shabestari S G. Effect of various melt and heat treatment conditions on impact toughness of A356 aluminum alloy. Transactions of Nonferrous Metals Society of China, 2016, 26: 956–965.
[12] Zhu M, Jian Z, Yang G, et al. Effects of T6 heat treatment on the microstructure, tensile properties, and fracture behavior of the modified A356 alloys. Materials & Design, 2012, 36: 243–249.
[13] Qiu K, Wang R, Peng C, et al. Effects of Mn and Sn on microstructure of Al-7Si-Mg alloy modified by Sr and Al-5Ti-B. Transactions of Nonferrous Metals Society of China, 2015, 25: 3546–3552.
[14] Liao H, Sun Y, Sun G. Restraining effect of strontium on the crystallization of Mg_2Si phase during solidification in Al-Si-Mg casting alloys and mechanisms. Materials Science and Engineering A, 2003, 358: 164–170.
[15] Pedersen L, Arnberg L. The effect of solution heat treatment and quenching rates on mechanical properties and microstructures in AlSiMg foundry alloys. Metallurgical and Materials Transactions A, 2001, 32A: 525–532.
[16] Jahangiri A, Marashi S P H, Mohammadaliha M, et al. The effect of pressure and pouring temperature on the porosity, microstructure, hardness and yield stress of AA2024 aluminum alloy during the squeeze casting process. Journal of Materials Processing Technology, 2017, 245: 1–6.
[17] Huang H, Fu P, Wang Y, et al. Effect of pouring and mold temperatures on hot tearing susceptibility of AZ91D and Mg-3Nd-0.2Zn-Zr Mg alloys. Transactions of Nonferrous Metals Society of China, 2014, 24: 922–929.
[18] Iben H M, Nadot Y, Fathallah R, et al. Influence of casting defect and SDAS on the multiaxial fatigue behaviour of A356-T6 alloy including mean stress effect. International Journal of Fatigue, 2015, 80: 90–102.
[19] Gunduz M, Kaya H, Cadirli E, et al. Interflake spacings and undercoolings in Al-Si irregular eutectic alloy. Materials Science and Engineering A, 2004, 369: 215–229.
[20] Grugel R, Kurz W. Growth of interdendritic eutectic in directionally solidified Al-Si alloys. Metallurgical and Materials Transactions A, 1987, 18A:1137–1142.
[21] Easton M A, Davidson C A, Stjohn D A. Effect of alloy composition on the dendrite arm spacing of multicomponent aluminum alloys. Metallurgical and Materials Transactions A, 2010, 41(6): 1528–1538.
[22] Martinez R A, Flemings M C. Evolution of particle morphology in semisolid processing. Metallurgical and Materials Transactions A, 2005, 36(8): 2205–2210.
[23] Yu L, Liu X, Wang Z, et al. Grain refinement of A356 alloy by AlTiC/AlTiB master alloys. Journal of Materials Science, 2005, 40: 3865–3867.
[24] Hu X, Xie L. Studies on the digital expression of Al-Si alloy microstructure and its applications in properties analysis. International Conference on Digital Manufacturing & Automation, Changsha, 2010: 427–431.

This work was supported by the Natural Science Foundation of Shandong Province (ZR2016EEM48).